LAWRENCE
LIVERMORE
NATIONAL
LABORATORY

LLNL-JRNL-636049

Transport of Electron Beams with Initial Transverse-Longitudinal Correlation

J. R. Harris, J. W. Lewellen, B. R. Poole

May 3, 2013

Journal of Applied Physics

Disclaimer

Transport of Electron Beams with Initial Transverse-Longitudinal Correlation

J.R. Harris*

Department of Electrical and Computer Engineering,
Colorado State University, Fort Collins, CO 80523

J.W. Lewellen

Los Alamos National Laboratory, Los Alamos, NM 87545

B.R. Poole

Lawrence Livermore National Laboratory, Livermore, CA 94550

ABSTRACT

When an electron beam whose current varies in time is extracted from a DC gun, the competition between the time-dependent space charge force and the time-independent focusing force will cause a correlation between radius, divergence, current, and position along the beam. This correlation will determine the beam's configuration in trace space, and together with the design of the downstream transport system, will determine the quality of the transport solutions that can be obtained, including the amplitude of the mismatch oscillations occurring in each slice of the beam. Recent simulations of a simplified diode with Pierce-type focusing operating at nonrelativistic voltages indicated that the radius and divergence of beams extracted from such guns can be approximated to high accuracy as linear functions of current. Here, we consider the impact of this dependence on the beam configuration in trace space and investigate the implications for matching and transport of such correlated beams in uniform linear focusing channels.

* Corresponding author. Electronic mail: john.harris@colostate.edu.

1. Introduction

DC electron guns use a constant voltage applied across a vacuum gap to accelerate a beam of electrons. As the beam travels through the gun, space charge will drive it to expand radially, and in many guns this expansion is offset by electrostatic focusing produced by the shape of the cathode and anode. This often includes the use of a cathode shroud making a 67.5° angle with the beam, which was first introduced by Pierce [1] and is intended to cancel the space charge force at the beam's edge when the gun is operating at the space-charge limit; in practice this angle is often used as a starting point for further iteration of the gun design. The situation is more complicated when pulsed beams are used. Pulsed beams, by definition, operate partially or entirely below the space charge limit, where the standard Pierce geometry will overfocus the beam, and the resulting competition between the time-dependent space charge force and the time-independent focusing force will establish a correlation between the transverse and longitudinal properties of the beam [2]. As a result, each slice along the beam's length may adopt a different orientation in the trace space defined by the beam's radius r and slope $r' = dr / dz$, leading to a growth in the overall area occupied by the beam in trace space. The beam's distribution will continue to change as it is focused for injection into a transport channel. This can be used to minimize the beam's area in trace space prior to downstream acceleration, a process known as emittance compensation [3,4]. However, when a low-energy, high-current beam is injected into a transport channel, the beam will continue to evolve under the influence of space charge while in the channel, and therefore will not retain its emittance-compensated configuration. The transverse-longitudinal correlation imposed on the beam by the gun and the focusing elements used to match it into the transport channel is still of critical importance, though, as it will determine the initial conditions of each slice of the beam at injection into the

channel. Even in the absence of initial transverse-longitudinal correlation, beams with variation in current that are transported through focusing channels will generally experience mismatch oscillations, and transverse-longitudinal coupling occurring inside the gun further complicates these effects. Transverse mismatch formed in this way will affect longitudinal expansion [5] and space charge wave propagation [6] along the beam in ways that can be sensitive to the details of the transport channel [5], and in a worst case scenario can lead to beam loss [7,8].

As a first step in studying these effects, we recently undertook a simulation study of transverse-longitudinal correlations occurring in a simplified DC electron gun [2]. We found that the beam radius and divergence at the anode could be closely described as linear functions of beam current over a very wide range of gun geometries and currents, and that the parameters of those linear functions depended on the gun geometry. Here we are primarily concerned with the consequences of this correlation on the beam's properties at extraction from the gun and on its injection and transport through a focusing channel. We will briefly review our previous simulation results, and will parameterize the beam's orientation and the area occupied by it in trace space. This is followed by considering the injection of these beams into transport channels, and the nature of the resulting mismatch oscillations. Throughout the paper, we will assume an intense electron beam whose current changes slowly compared to its transit time across the diode, and in which longitudinal evolution of the beam is neglected.

2. Review of Simulation Results.

For our previous study of transverse-longitudinal correlation, discussed in detail in Ref. [2], we chose a DC gun using a Pierce-like geometry, a 4 mm radius planar emissive surface, and a 16 mm radius anode and cathode (Figure 1). Simulations were performed for cases with cathode shroud angles (θ) between 50° and 100°, anode-cathode distances (d_{AK}) between 10

mm and 40 mm, and anode-cathode voltages (V_{AK}) between 500 V and 20 kV using the codes CST Particle Studio (CST-PS) [9], TRAK [10], and SPIFFE [11]; all three codes gave similar results. Several simplifications were incorporated in this geometry. First, it did not include a control grid due to the complexity of the behavior associated with control grids and our desire to focus on other aspects of gun performance. In addition, while no anode aperture is included, this geometry approximates the internal electrostatic configuration of a gun in which an anode grid is used to prevent aperture defocusing of the extracted beam. Our geometry also departs from the ideal Pierce geometry by the absence of a shaped anode, but in practice the primary focusing effect is provided by the cathode and anode shaping is often ignored. We assumed that the current changed slowly compared to its transit time across the anode-cathode gap. Figure 2 shows the effect of cathode shroud angle and anode-cathode distance on the radius and divergence of the beam arriving at the anode, using results obtained from CST-PS with an anode-cathode voltage of 10 kV. Figure 2 also shows the results of linear regressions to the simulation results, demonstrating that the beam radius and divergence can be modeled well as linear functions of current, and that the slope and intercept of those linear functions depend on the gun geometry. Figure 3 shows representative configurations for the simulated beam arriving at the anode, for several combinations of cathode angle and anode-cathode distance. In this figure, we have added lines to the origin from the peak-current ("P") and zero-current ("0") slices, and reflected the geometry through the origin to make the entire area occupied by the beam in trace space more clear.

3. Trace Space Configuration and Gun Geometry.

The observed linear dependence on current of the beam's radius and divergence can be used to explain the shape of the distributions in Figure 3, and allows the area occupied by the beam in trace space to be easily calculated. Let us express the beam radius at the anode as

$$r(I) = a_0 + a_1 I \tag{1}$$

and express the divergence at the same location as

$$r'(I) = b_0 + b_1 I\,. \tag{2}$$

These equations can be combined to give

$$r' = \left(\frac{b_1}{a_1}\right) r + \left(b_0 - \frac{a_0 b_1}{a_1}\right), \tag{3}$$

which defines a line in trace space along which the radius and divergence of each slice of the beam must fall (Figure 4). This line will be populated between a point (a_0, b_0), establishing the orientation of the zero-current slice, and a point $(a_0 + a_1 I_{pk}, b_0 + b_1 I_{pk})$, establishing the orientation of the slice containing the peak current (I_{pk}). These two points and the origin define a region whose area is one-half of the total area A_r occupied by the beam in trace space, given by

$$A_r = I_{pk} \left| a_1 b_0 - a_0 b_1 \right|. \tag{4}$$

The quantity A_r / π can be considered to be an effective emittance. However, it is based on an unweighted area in trace space, and is therefore different than the weighted area in trace space used to calculate the more common RMS emittance [12]. The projected RMS emittance will differ from A_r / π depending on how the beam current varies as a function of time. But because our objective is to study the effects of gun geometry, rather than those due to the current pulse shape, it is more appropriate to use the trace space area defined above than an RMS

emittance. The trace space area of Eq. (4) can still be viewed as a gun-geometry-dependent, pulse-shape-independent measure of the worst case projected emittance in any particular gun.

Following this approach, the linear fitting functions shown in Figure 2 were used to define the coefficients a_n and b_n describing the simulated beam configurations at the anode. These coefficients, shown in Tables I and II, were then used to calculate the area occupied by the beam in trace space, using Eq. (4) and taking the space charge limited current for each geometry as I_{pk}. The results are shown with the black diamonds in Figures 5 and 6. These results indicate that the area occupied in trace space decreased as the focusing angle decreased and as the anode-cathode distance increased. However, Eq. (4) shows that there are two inter-related, but different, factors determining the trace space area. The first is the gun geometry, which determines the coefficients a_n and b_n. The second is the peak current I_{pk}. The upper limit on I_{pk} is the space charge limited current I_{SCL}, which will also depend on gun geometry. However, the gun may be operated at lower peak currents, for example when operating in emission-limited mode to allow photoemission-modulation of the beam current [13]. In Figures 5 and 6 we assumed that the gun current was swept through its entire range, from zero to I_{SCL}. To isolate the direct effect of gun geometry when operating in emission-limited mode, we have also plotted $\left|a_1 b_0 - a_0 b_1\right|$ as a function of cathode angle in Figure 5 and as a function of anode-cathode distance in Figure 6 (red squares). This shows that the largest reduction in the *direct geometric contribution* to the trace space area is actually achieved by going to larger angles, and to smaller anode cathode distances. This is reasonable, as larger angles provide a better approximation of an ideal spherical diode, in which all electron trajectories would be radial, independent of current in the diode. Similarly, going to smaller gap lengths provides a better approximation of an ideal

parallel-plate diode, in which the electron trajectories would be rectilinear, independent of diode current. But larger cathode angles and smaller anode-cathode distances are also both associated with increases in the space charge limited current, which demonstrates that the two effects in Eq. (4) are competing when $I_{pk} = I_{SCL}$. Note that the space charge limited current found in our simulations and shown in Table II falls off more slowly with anode-cathode distance than predicted by multiplying the one-dimensional Child-Langmuir law [14, 15]

$$J = \frac{4}{9}\varepsilon_0 \left(\frac{2q}{m}\right)^{1/2} \frac{V_{AK}{}^{3/2}}{d_{AK}{}^{2}} \tag{5}$$

by the cathode area, $\pi r_K{}^2$, where ε_0 is the permittivity of free space, and q and m are the charge and mass of the electron. This is likely due to imperfect cancellation of the radial space charge force at the beam edge in our simplified geometry, leading to increased beam expansion as the anode-cathode distance is increased, as suggested by Figure 7. Also note that while the results presented here were obtained with an anode-cathode voltage of 10 kV, simulations performed at other (non-relativistic) voltages produce results for the radius and divergence as a function of fractional saturated current (I / I_{SCL}) which all fall along a single curve for a given geometry [2]. As a result, the zero-current coefficients a_0 and b_0 and the products $a_1 I_{pk}$ and $b_1 I_{pk}$ -- and therefore the area occupied by the beam in trace space -- must be independent of anode-cathode voltage.

4. Matching and Transport: "Well-Confined" Beams

When a beam is extracted from a gun with a constant current, radius, and divergence, it is relatively straightforward to match it into a transport channel with initial conditions that avoid mismatch oscillations. But the problem is much more challenging when the beam's current, radius, and divergence at extraction are all changing. In principle, matched transport of every

slice of the beam could be achieved in a uniform focusing channel, but this would require that every slice be injected into the channel with zero divergence and at its matched radius $r_{match}(I) = \sqrt{K}/k_0$, where k_0 is the linear focusing strength of the channel and $K = qI/2\pi\varepsilon_0 mc^3\beta^3\gamma^3$ is the generalized perveance which depends on the beam current I and energy in each slice [16]; unfortunately, this is a very difficult condition to generate. The question therefore becomes, not how can we *eliminate* mismatch oscillations, but rather how can we *accommodate* mismatch oscillations in an optimal way?

At the low energies we are considering here, a typical application of electron beams is microwave production through interaction with a slow wave structure. These microwave sources generally require tight coupling -- and therefore the minimum possible distance -- between the beam and the structure. This means that beam loss by scraping is a very real possibility, and so mismatch oscillations that might exceed the nominal beam radius must be avoided. As a result, we can adopt as our optimization criteria that 1) the peak-current slice is matched in the transport channel, and 2) the radius for all other slices remains less than that of the peak-current slice while in the channel. We will refer to this as a "well-confined" beam.

We can also establish a mathematical condition for well-confined beams by considering the radial energy of a particle at the beam edge. When a slice of the beam has just entered the uniform focusing channel -- which is assumed here to begin abruptly -- a particle at the edge of that slice will have a radial kinetic energy associated with its divergence, and a radial potential energy determined by its radius and the strengths of the competing space charge and focusing forces. If the sum of that radial kinetic energy and radial potential energy at injection into the channel is less than the radial potential energy the particle would have if its radius were equal to the channel design radius, then the radius of that slice will not exceed the channel design radius,

and will be well-confined by our definition. The radial potential energy is associated with the space charge force $qI/2\pi\varepsilon_0 c\beta\gamma^3 r$ and the focusing force $-k_0^2 c^2\beta^2 mr$ experienced by the particle, which will be equal -- therefore giving a minimum potential energy we define as zero -- when $r(I) = r_{match}(I)$. We are therefore concerned with the potential energy gained by a particle experiencing a radial displacement Δr away from that equilibrium radius, which is given by

$$U(\Delta r) = \int_0^{\Delta r} \left(\frac{qI}{2\pi\varepsilon_0 c\beta\gamma^3} \frac{1}{r_{match}(I)+\delta} - k_0^2 c^2\beta^2 m\left(r_{match}(I)+\delta\right) \right) d\delta . \tag{6}$$

Our requirement for well-confined transport of a beam injected with radius r_{inj} and divergence r_{inj}' into the focusing channel having a design radius r_{ch} becomes

$$\frac{1}{2} mc^2\beta^2 \left(r_{inj}'\right)^2 + U(r_{inj} - r_{match}) \le U(r_{ch} - r_{match}) , \tag{7}$$

or

$$\left(r_{inj}'\right)^2 \le 2K \ln\left(\frac{r_{inj}}{r_{ch}}\right) + k_0^2\left(r_{ch}^2 - r_{inj}^2\right). \tag{8}$$

Eq. (8) establishes the maximum and minimum divergence that a slice with current I and radius r_{inj} may have at injection into the channel and still be well-confined by our definition, and therefore imposes a limitation on the configurations the beam may exhibit at the entrance to the focusing channel. For the peak current slice, injection occurs at $r_{inj} = r_{ch}$, so that the entire energy budget for that slice is expended in the form of potential energy, requiring $r_{inj}' = 0$ as expected. The issue now becomes finding a matching system which takes a beam with initial transverse-longitudinal correlation from the gun and manipulates it so that it meets the requirement of Eq. (8) when arriving at the transport channel.

5. Matching and Transport: Numerical Calculation

To search for configurations providing well-confined beams, we chose a simple transport system consisting of a 5 cm long matching solenoid, followed by a single long solenoid (Figure 8). Ten beam slices -- with currents of 100%, 90%, 80%, 60%, 40%, 20%, 10%, 5%, 1%, and 0.1% of the peak current -- were launched into this system using initial conditions defined by Eqs. (1) and (2) and Tables I and II [17], and the evolution of each slice was found by numerical integration of the envelope equation [12]

$$r''(z) + k_0^2(z)r(z) - \frac{K}{r(z)} - \frac{\varepsilon^2}{r^3(z)} = 0. \qquad (9)$$

For comparison, we also considered a beam launched with no initial correlation, in which the initial radius of 4 mm and divergence of zero were independent of current. To isolate the effects of the initial transverse-longitudinal correlation, rather than differences in peak current produced by the different gun configurations, we assumed a peak current of 0.218 A in all cases, which is equal to the lowest space charge limited current of the simulated cases. Two focusing strengths were chosen for the long solenoid, which provided a matched beam radius of 5 mm ($k_0 = 11.427\text{m}^{-1}$) or 2 mm ($k_0 = 28.567\text{m}^{-1}$) for the 0.218 A slice. An emittance of $\varepsilon = 10^{-6} m$ was used in order to provide realistic treatment of low current slices near waists.

The transport system therefore had three free parameters: 1) the beam initial conditions, 2) the matching solenoid location, and 3) the long solenoid strength. Because our objective was to provide matched transport for the peak-current slice in each case, fixing these three parameters also determined the matching solenoid strength and the distance between the matching and long solenoids. To systematically search through this parameter space, a location l_{sol} for the matching solenoid was first chosen, and the matching solenoid strength k_{sol} and long solenoid location were adjusted to bring the peak-current slice to a waist with the desired channel radius

r_{ch} (5 mm or 2 mm) at the entrance to the long solenoid. The effectiveness of the beam transport for all slices was considered, and then the matching solenoid location was iterated by 0.5 cm or 1 cm. This process was repeated for each combination of initial conditions and long solenoid strengths. For the figures in this paper, the location of the solenoid was referenced to the solenoid center, as indicated with the back arrow in Figure 8.

Figure 8 also shows typical envelopes obtained in this way. Part a shows a threshold case, where the radius of the 0.218 A slice has just reached the desired 5 mm radius inside the matching solenoid. Moving the matching solenoid farther left would not allow for matched injection of this slice because its radius would be too small at the matching solenoid. Part b shows an example of a channel configuration providing a typical well-confined beam, while part c shows a case where the beam is not well-confined according to our definition.

Figure 9 shows a comparison between the results from Figure 8 and the predictions of Eq. (8). The orientation in trace space of the 100%, 80%, 20%, and 0.1% current slices at the entrance of the long solenoid is shown, for matching solenoid locations as shown in Figure 8. The dotted contours are generated from Eq. (8), and indicate the allowable orientations for slices with 80%, 20%, and 0.1% of the peak current. No contour is shown for the 100% case because Eq. (8) requires the peak current slice to be injected into the long solenoid with zero divergence. In cases a and b, all endpoints fall within the corresponding contours, indicating that well-confined transport is predicted by Eq. (8). In case c, the endpoints for the 80% and 20% slices fall outside their corresponding contours, indicating that well-confined transport is not predicted by Eq. (8). Both predictions are in agreement with the results shown in Figure 8.

Notice that for each value of slice current, the allowable range of injection radii is maximized when the divergence for that slice is zero, which is also the requirement for emittance compensation.

The results obtained from our procedure for all geometries and initial conditions where well-confined transport was achieved are summarized in Figure 10. None of the tested cases produced well-confined transport when the focusing strength was adjusted for a 2 mm design radius, and therefore all cases shown in Figure 10 are for injection into a 5 mm channel. The curves in that figure show the matching solenoid strength k_{sol} required to match the peak current slice into the long solenoid as a function of the matching solenoid location l_{sol}. No data is shown to the left of the vertical dashed line at 2.5 cm, as this line corresponds to the minimum distance between the center of the 5 cm long matching solenoid and the gun extraction plane. In the other cases where the curves end, no matching solution was found for the peak current slice because its radius was smaller than channel design radius at the location of the matching solenoid. Where dotted lines are shown, the peak current slice was properly matched into the channel, but the radii of other slices exceed that of the peak current slice, as shown in Figure 8c, so that the transport was not well-confined by our definition. Where solid lines are shown, the peak current slice was properly matched into the channel, and all other slices had radii that never exceed the design radius, as in Figure 8a and 8b, and are therefore well-confined.

Figure 10 clearly shows that the initial transverse-longitudinal correlation introduced onto the beam by the choice of gun geometry strongly influences the nature and quality of matching solutions. The case with no initial correlation produced a well-confined beam using the lowest matching solenoid strength of any case. The presence of an initial correlation generally increased the required matching solenoid strength, but also generally increased the range of

solenoid locations providing well-confined beams. Providing well-confined beams at smaller solenoid locations allows the system to be designed for both lower beam interception and shorter system length. Notice that by going to a 70° cathode angle rather than the nominal 67.5° angle, the range over which well-confined beams could be produced was significantly increased, but that this improvement is quickly lost by going to a 75° angle. None of the other cases in Table I were able to produce well-confined beams. Also note that smaller anode-cathode distances, which provide less opportunity for radial expansion of the beam in the gun and therefore a weaker initial correlation, generally provide results that are more similar to the hypothetical case with no transverse-longitudinal correlation. However, the range over which the solutions could be found providing well-confined beams also generally decreases as the anode-cathode distance is decreased, to the point that no such solutions were found for the 10 mm and 15 mm cases.

5. Summary

When a pulsed beam is extracted from a DC electron gun, the competition between the time-dependent space charge force in the beam and the time-independent focusing force produced by the gun will result in a correlation between the transverse and longitudinal properties of the beam. Our previous simulation study of this effect indicated that this correlation caused a linear dependence of the beam radius and divergence on the beam current. Here, we reviewed these simulations and presented new results for the first time. We then used this linear dependence to parameterize the beam's orientation and area occupied in trace space, and to identify and study the competing direct and indirect geometric effects controlling them. We also considered the injection of these beams into uniform focusing channels using a matching section consisting of a single short solenoid, and introduced an optimization criterion for transport of beams with initial transverse-longitudinal correlation and varying current through

this system. For each of the simulated gun configurations, we searched for matching solenoid locations and strengths which satisfied this optimization criterion. The range of matching solenoid locations over which satisfactory transport could be obtained depended on the gun geometry. Placement of the matching solenoid closer to the gun was preferred, often providing both optimized transport and lower required focusing strengths for this solenoid, as long as the solenoid was far enough away from the gun to allow expansion of the beam to the desired channel radius before reaching the solenoid. Satisfactory transport solutions were found for most gun configurations for channel design radii of 5 mm, but none were found for channel radii of 2 mm. Note that because a 4 mm cathode radius was used in these simulations, the beam's current density in the 5 mm channel would be less than at the cathode. Conversely, the current density in the 2 mm channel would be larger than that at the cathode, as is generally preferred in microwave sources. It remains unclear whether "well-confined" transport as defined here is fundamentally incompatible with current density compression ratios greater than 1. For the 5 mm channel radius, satisfactory transport solutions were found for a wide range of anode-cathode distances, but the range of acceptable focusing angles was fairly small.

ACKNOWLEDGEMENTS

This work was primarily funded by the Office of Naval Research and the High Energy Laser Joint Technology Office, with additional work performed under the auspices of the U.S. Department of Energy by Lawrence Livermore National Laboratory under Contract DE-AC52-07NA27344.

REFERENCES

[1] J.R. Pierce, Journal of Applied Physics **11,** 548 (1940).

[2] J.R. Harris, J.W. Lewellen, and B.R. Poole, Journal of Applied Physics **112**, 023304 (2012).

[3] B.E. Carlsten, Nuclear Instruments and Methods A **285**, p. 313-319 (1989).

[4] L. Serafini and J.B. Rosenzweig, Physical Review E **55,** 7565-7590 (1997).

[5] J.R. Harris, R.B. Feldman, and P.G. O'Shea, "Transverse-Longitudinal Coupling in an Intense Electron Beam," in Proceedings of the 2007 Particle Accelerator Conference, p. 3597-3599. Online: http://accelconf.web.cern.ch/AccelConf/p07/PAPERS/THPAS046.PDF

[6] B.R. Poole, D.T. Blackfield, Y.-J. Chen, J.R. Harris, and P.G. O'Shea, "Space Charge Waves in Mismatched Beams," in Proceedings of the 2009 Particle Accelerator Conference, p. 3272-3274. Online: http://accelconf.web.cern.ch/AccelConf/PAC2009/papers/th5pfp035.pdf

[7] J.R. Harris and P.G. O'Shea, Physics of Plasmas **15**, 123106 (2008)

[8] J.R. Harris and J.W. Lewellen, Journal of Applied Physics **108**, 083301 (2010).

[9] H. Spachmann and U. Becker, Nuclear Instruments and Methods A **558,** 50-53 (2006).

[10] S. Humphries, Journal of Computational Physics **125**, 488-497 (1996).

[11] M. Borland, "Summary of Equations and Methods used in SPIFFE," APS/ IN/LINAC/92-2, 29 June 1992.

[12] M. Reiser, *Theory and Design of Charged Particle Beams*, Wiley: New York (2008).

[13] J.R. Harris, J.G. Neumann, and P.G. O'Shea, Journal of Applied Physics **99**, 093306 (2006).

[14] C.D. Child, Physical Review (Series I) **32**, 492-511 (1911).

[15] I. Langmuir, Physical Review (Series II) **2**, 450 (1913).

[16] This may be considered as a special case of emittance compensation, which generally requires only that each slice has zero divergence.

[17] This effectively assumes that the beam passed through a gridded aperture in the anode and neglects beam loss associated with the anode grid, a satisfactory approximation for the purposes of this study.

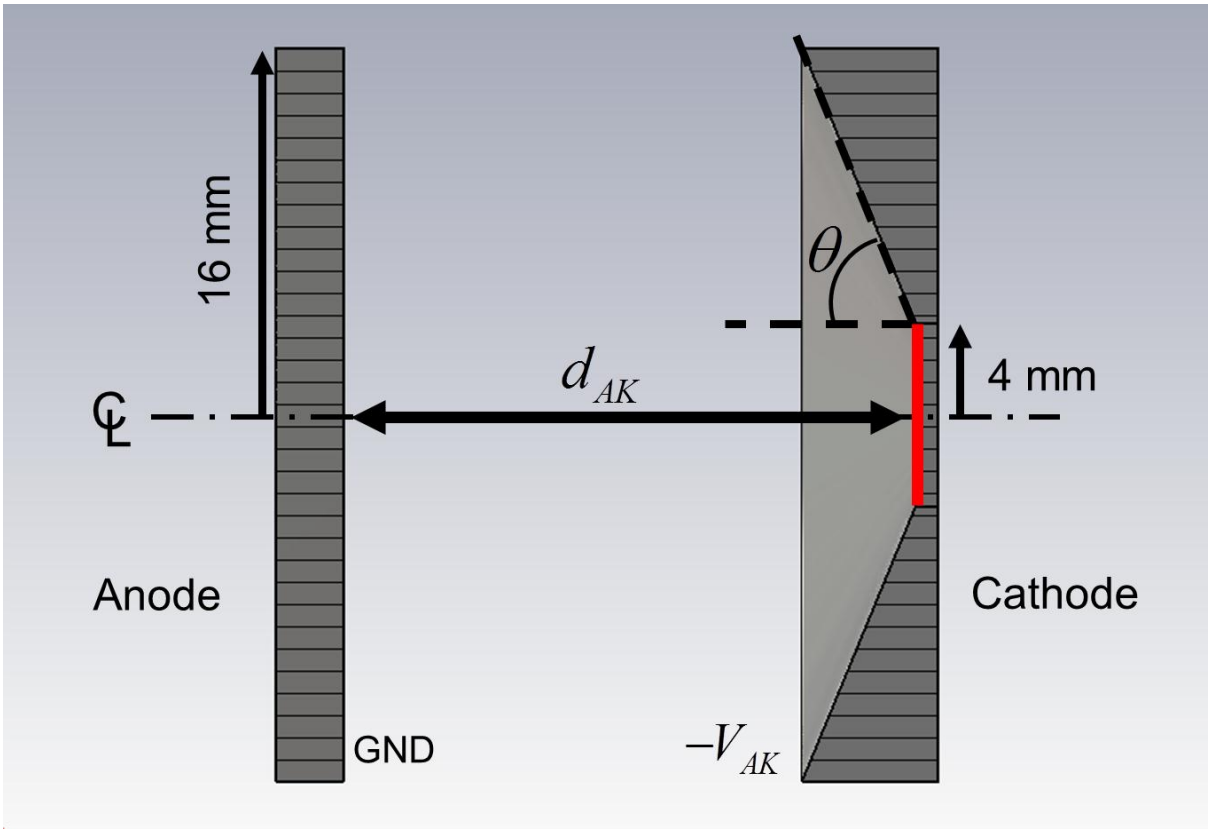

Figure 1. Drawing of the simulated electron gun, with the cathode emissive surface indicated in red and the system centerline denoted by ℄.

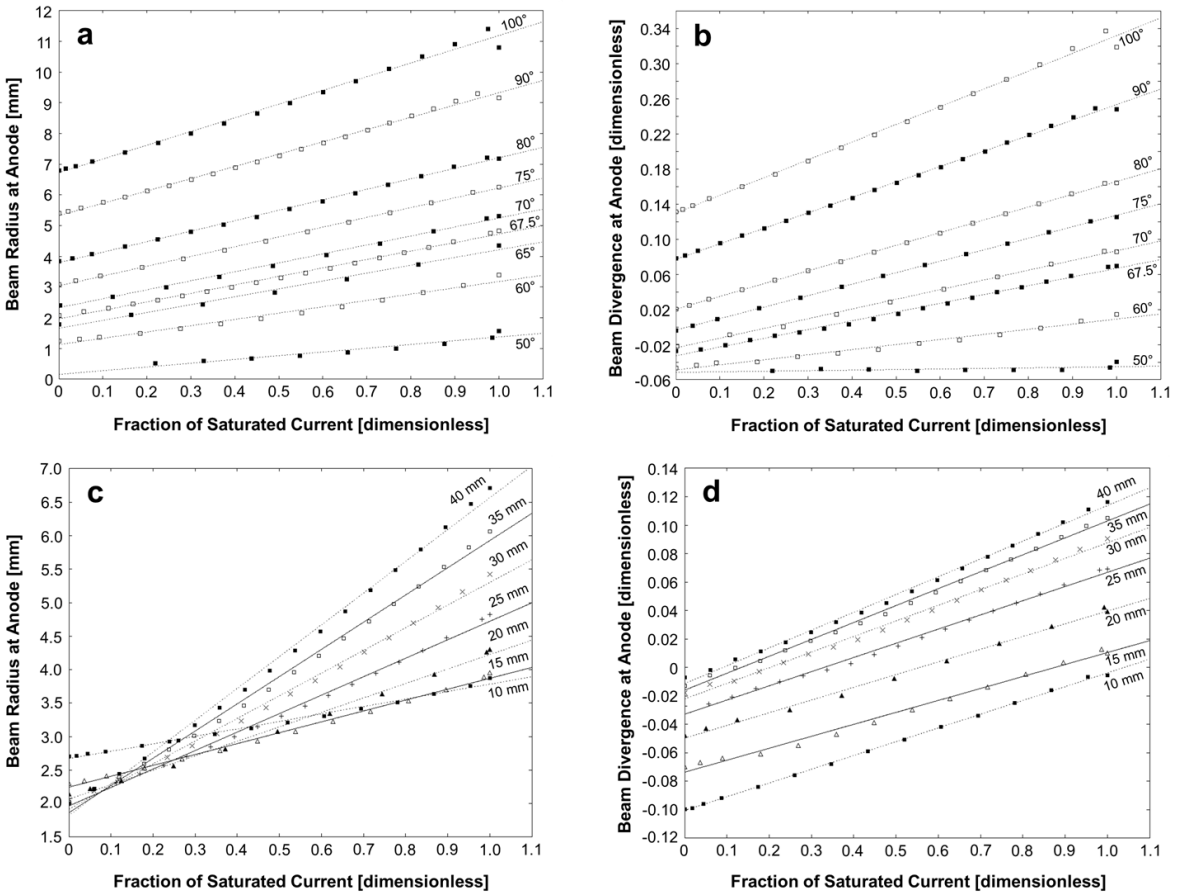

Figure 2. Beam radius and divergence at the anode as a function of beam current (expressed as the fraction of the space-charge-limited current I / I_{SCL}) for several geometries: a) and b) show the effect of cathode angle assuming a 25 mm anode-cathode distance, while c) and d) show the effect of anode-cathode distance assuming a cathode angle of 67.5°. Anode-cathode potential of 10 kV is used in all cases. Fitting functions are linear, and alternate data series are shown with different symbols for clarity.

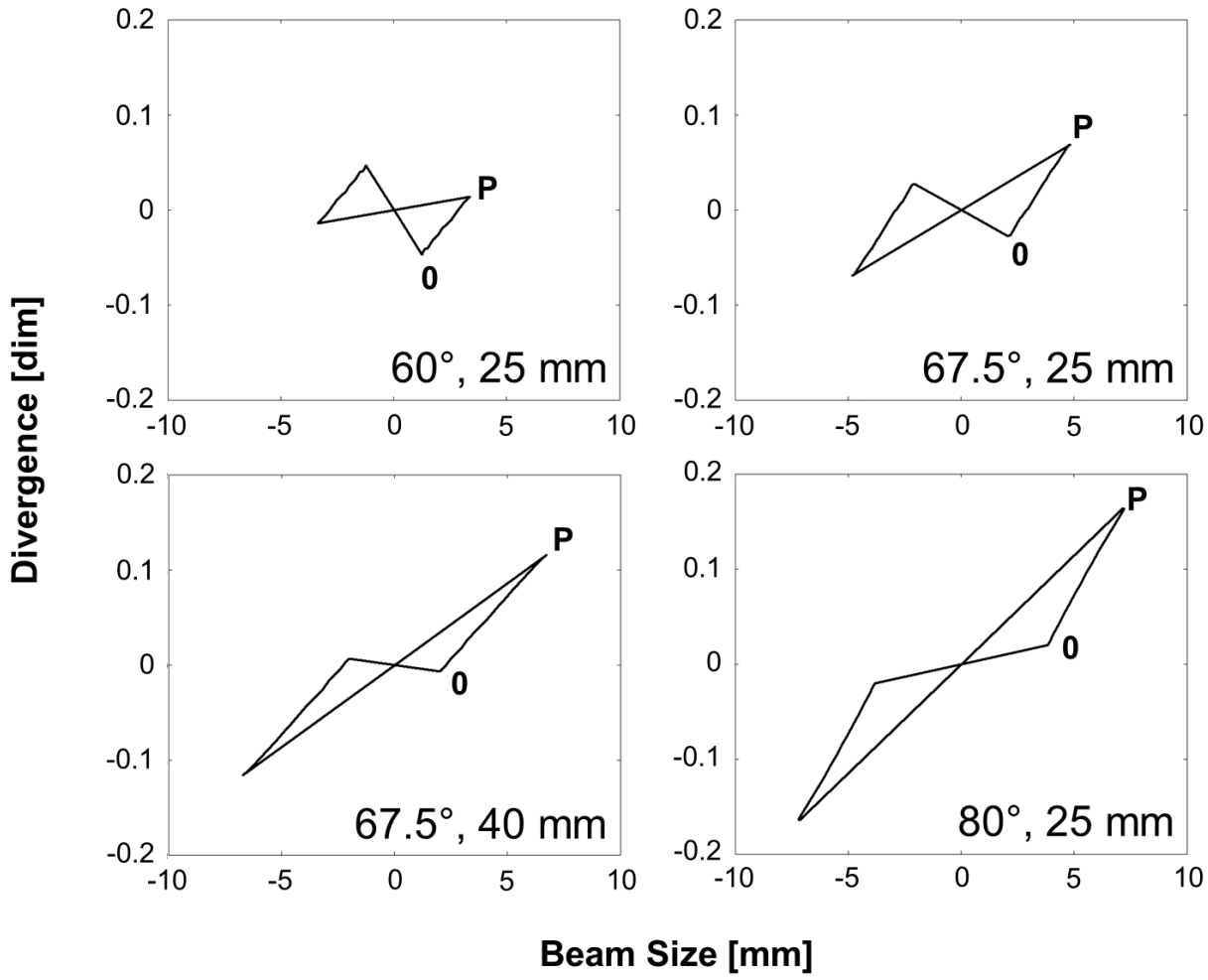

Figure 3. Trace space plots for a beam arriving at the anode in an electron gun with an anode-cathode voltage of 10 kV for various cathode angles and anode-cathode distances. The zero-current and peak-current slices are denoted by "0" and "P," respectively.

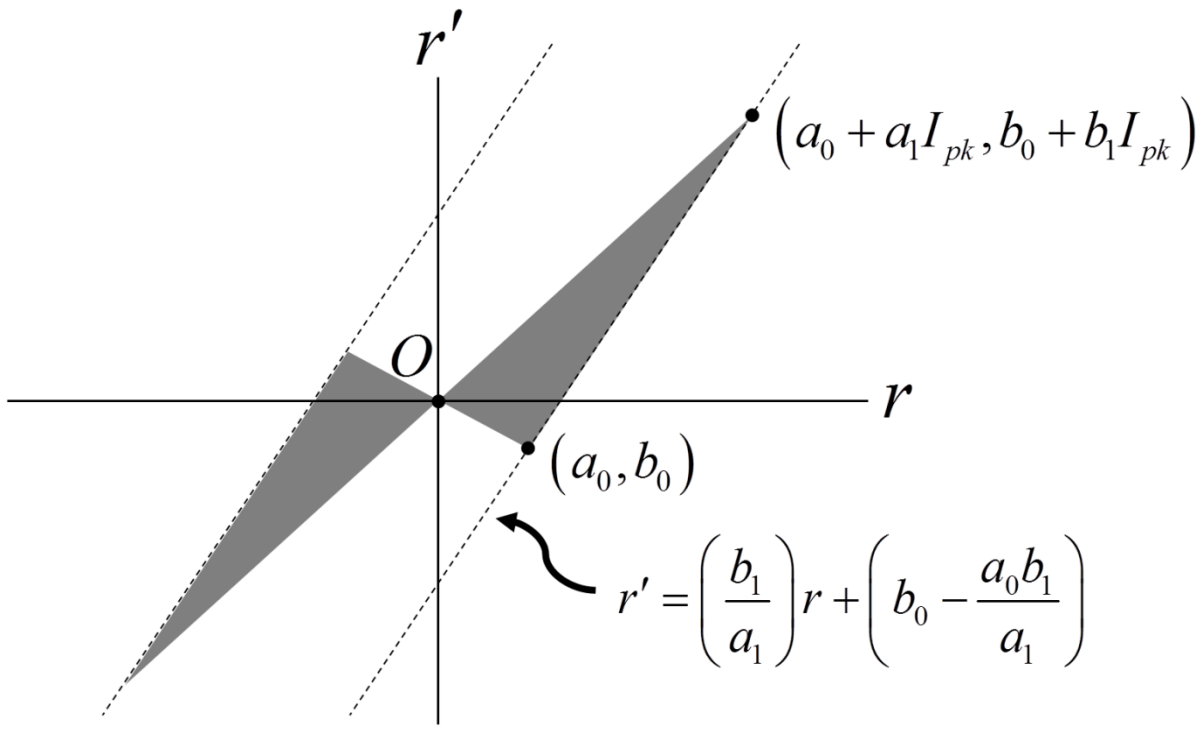

Figure 4. Trace space construction.

Table I. Linear regression coefficients for beam arriving at the anode of the simulated diodes with anode-cathode voltage of 10 kV and anode-cathode distance of 25 mm. I_{SCL} is the space-charge limited current for each configuration, found using CST-PS. Trace space areas listed here are calculated using Eq. (4) and taking $I_{pk} = I_{SCL}$. All values were rounded to three significant figures after calculation.

Angle [deg]	a_0 [m]	a_1 [m/A]	b_0 [dim]	b_1 [A^{-1}]	I_{SCL} [A]	A_r [μm]
60	0.00112	0.00943	-0.0492	0.267	0.218	166
67.5	0.00196	0.00772	-0.0330	0.279	0.357	287
70	0.00232	0.00710	-0.0239	0.269	0.411	327
75	0.00304	0.00598	-0.00372	0.246	0.532	408
80	0.00379	0.00511	0.0202	0.218	0.668	483
90	0.00532	0.00400	0.0770	0.177	0.998	631
100	0.00672	0.00335	0.130	0.152	1.33	779

Table II. Linear regression coefficients for beam arriving at the anode of the simulated diodes with anode-cathode voltage of 10 kV and focusing electrode angle of 67.5°. I_{SCL} is the space-charge limited current for each configuration, found using CST-PS. Trace space areas listed here are calculated using Eq. (4) and taking $I_{pk} = I_{SCL}$. All values were rounded to three significant figures after calculation.

Distance [mm]	a_0 [m]	a_1 [m/A]	b_0 [dim]	b_1 [A^{-1}]	I_{SCL} [A]	A_r [μm]
10	0.00267	0.000966	-0.101	0.0838	1.15	371
15	0.00224	0.00291	-0.0737	0.151	0.558	308
20	0.00206	0.00535	-0.0498	0.221	0.403	292
25	0.00196	0.00772	-0.0330	0.279	0.357	287
30	0.00192	0.00989	-0.0213	0.317	0.342	280
35	0.00186	0.0120	-0.0160	0.353	0.337	287
40	0.00182	0.0141	-0.0114	0.373	0.335	281

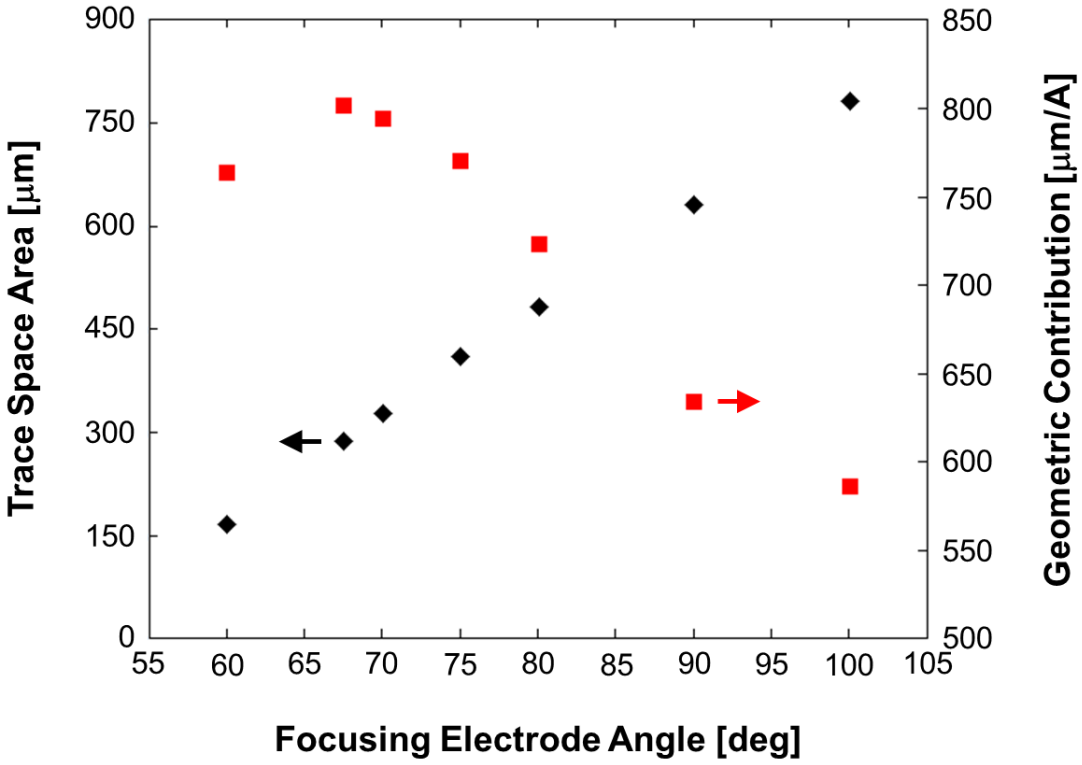

Figure 5. Dependence of trace space area (black diamonds) and the geometric contribution to trace space area ($|a_1 b_0 - a_0 b_1|$, red squares) on focusing electrode angle for the simulated cases, using an anode-cathode distance of 25 mm and an anode-cathode voltage of 10 kV, calculated using the results in Table I.

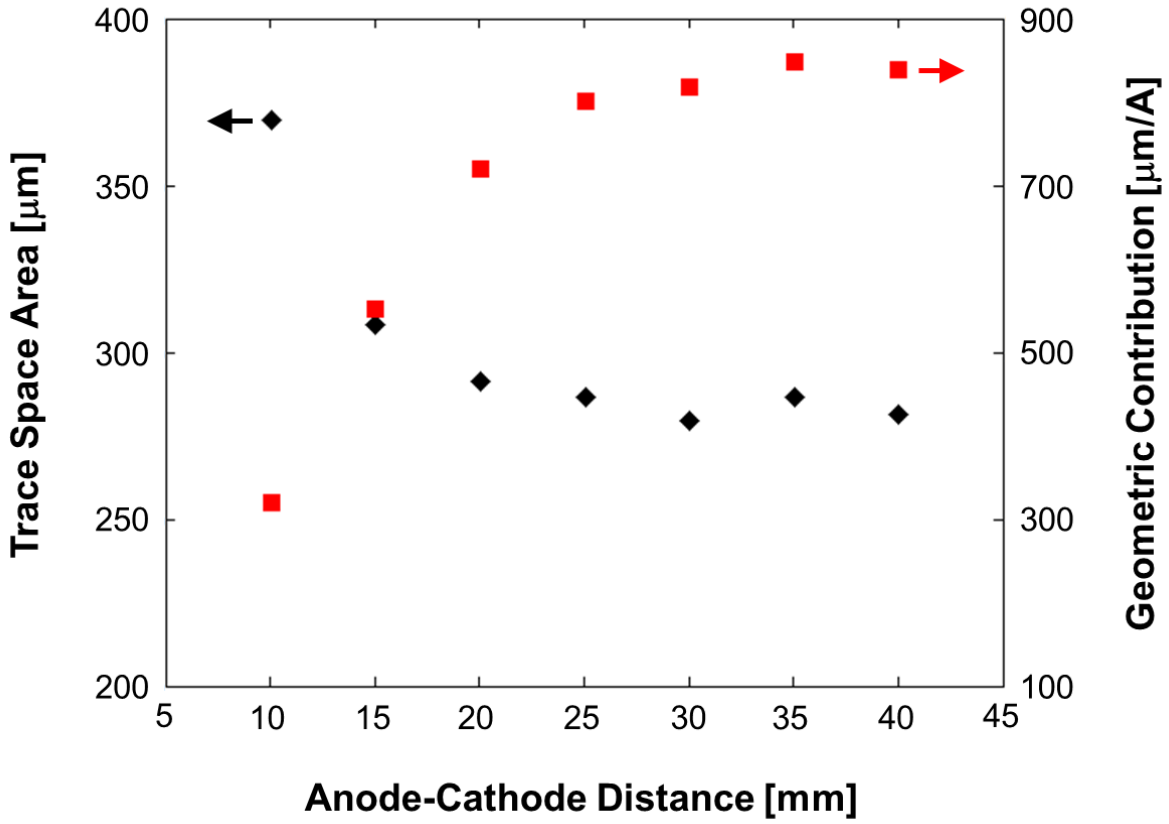

Figure 6. Dependence of trace space area (black diamonds) and the geometric contribution to trace space area ($|a_1 b_0 - a_0 b_1|$, red squares) on anode-cathode distance for the simulated cases, using a focusing electrode angle of 67.5° and an anode-cathode voltage of 10 kV, calculated using the results in Table II.

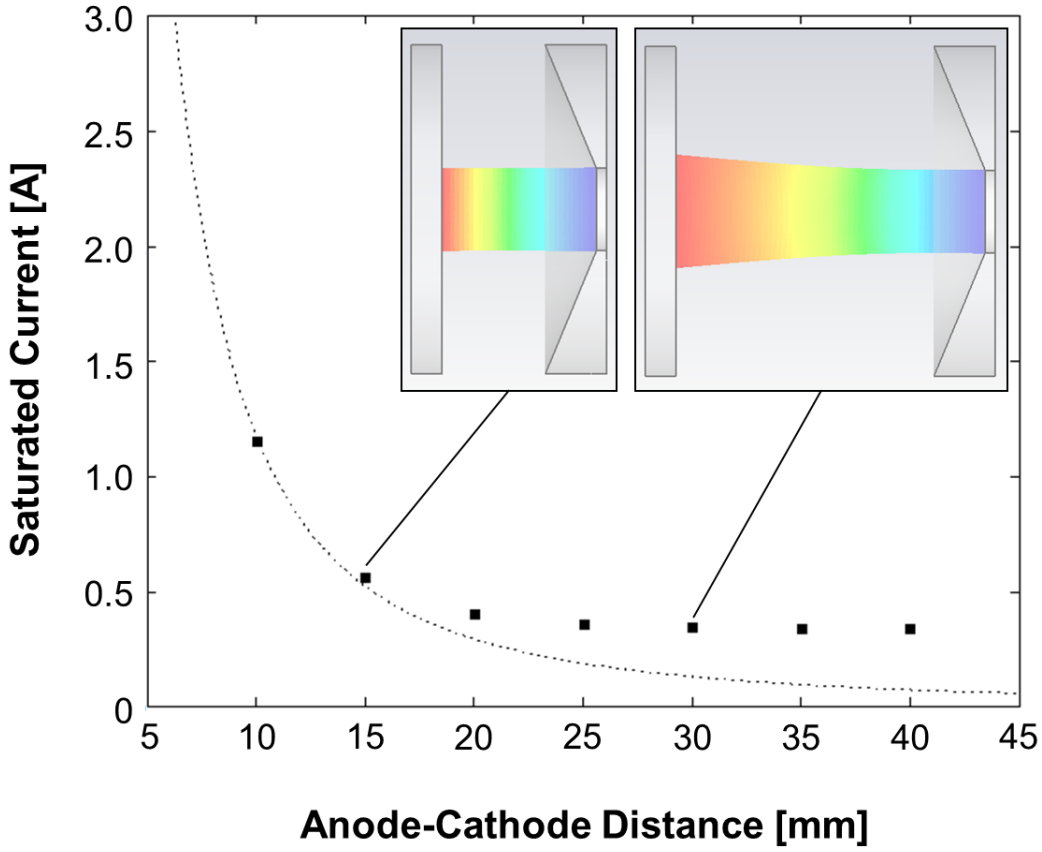

Figure 7. Space charge limited current as a function of anode-cathode distance from Table II for the simplified diode with anode-cathode potential of 10 kV and a cathode angle of 67.5°. The dotted line is generated by multiplying the current density predicted by the Child-Langmuir equation by the cathode surface area. The insets show the space-charge limited beam envelopes for the 15 mm and 30 mm spacings. This curve agrees well with the CST-PS simulation results for small anode-cathode distances in which the beam divergence at the anode is minimal, but for larger distances the beam expands transversely, allowing transmission of larger currents than predicted by a simple application of the Child-Langmuir law.

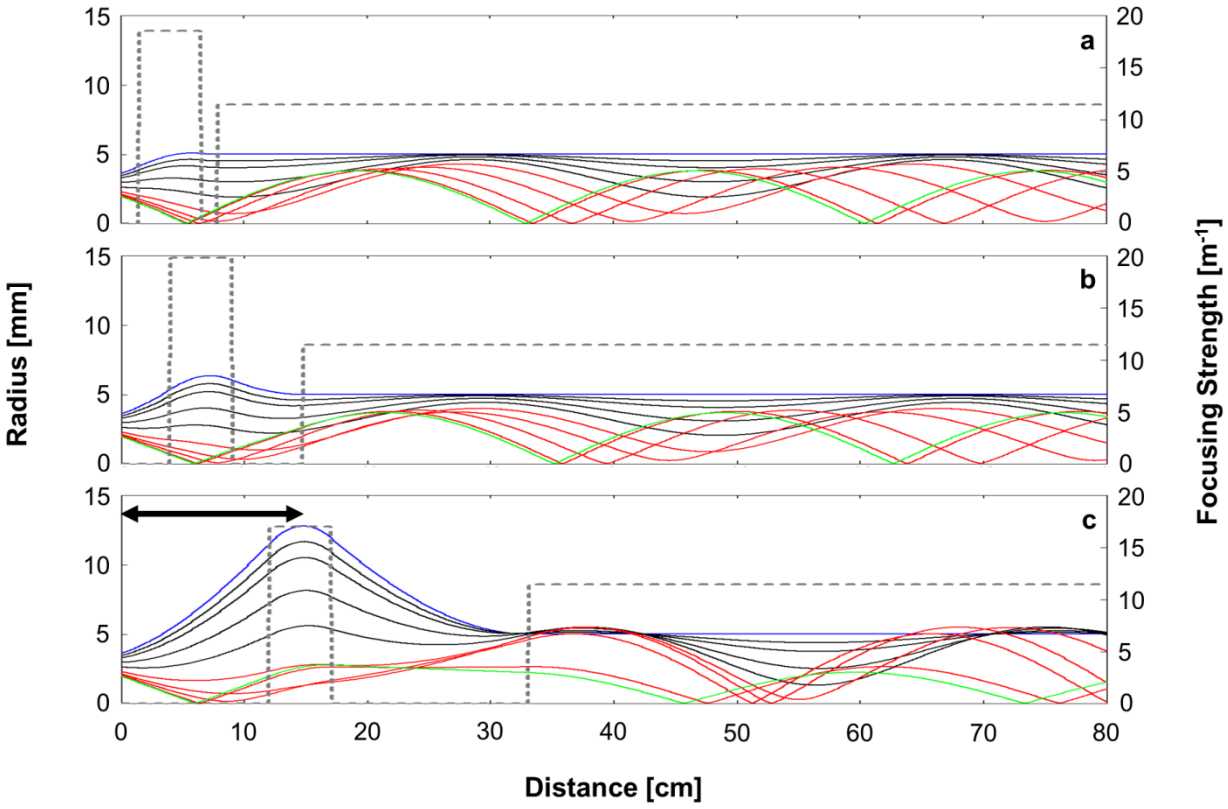

Figure 8. Typical results from envelope calculation, in this case for a beam with initial conditions corresponding to the 67.5°, 25 mm case, with a peak current of 0.218 A being matched into a channel with 5 mm radius. The dotted gray line indicates the focusing strength, while the solid curves represent the evolution of the peak current (blue), 0.1% current (green), higher current (black), and lower current (red) slices of the beam. Three cases are shown: a) the threshold case for matching of the peak current slice (l_{sol} = 4 cm, k_{sol} = 18.55 m^{-1}); b) a case where the beam is "well-confined" (l_{sol} = 6.5 cm, k_{sol} = 19.79 m^{-1}); and c) a case where the beam is not "well-confined" (l_{sol} = 14.5 cm, k_{sol} = 17 m^{-1}).

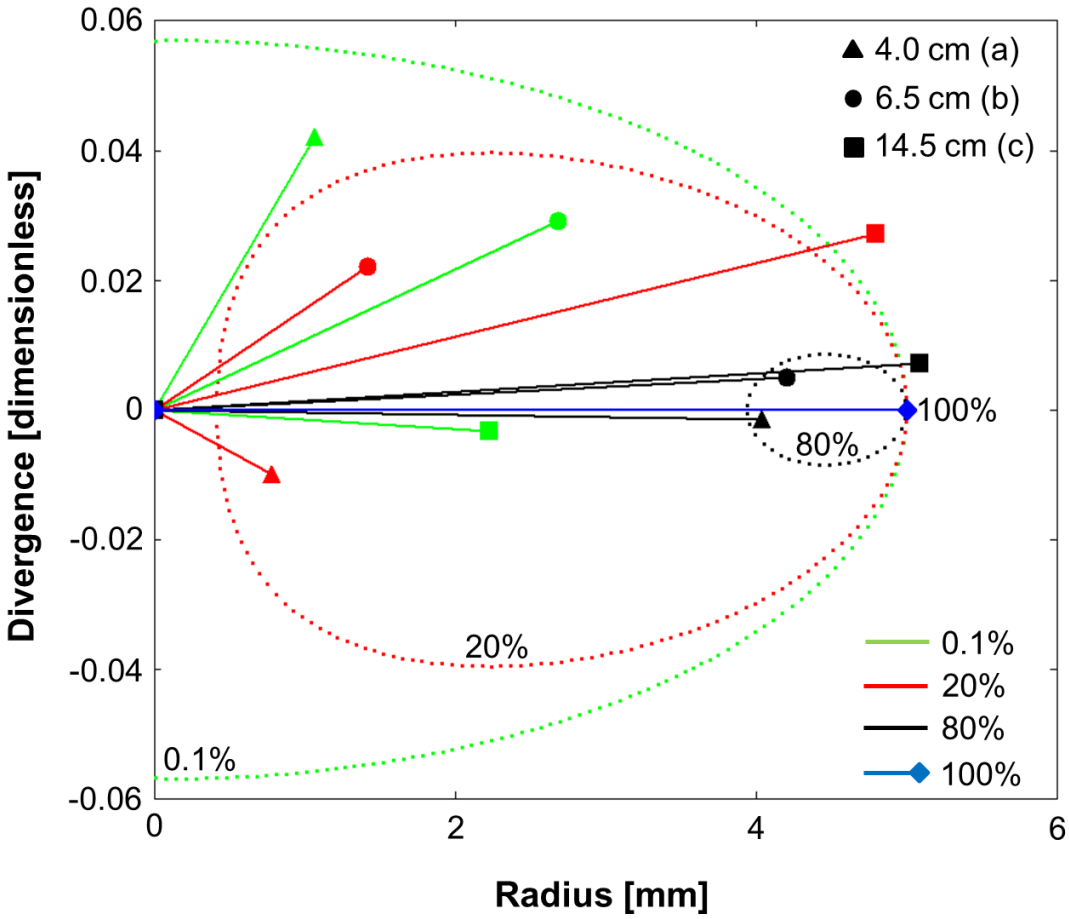

Figure 9. Trace space configurations at entrance into the long solenoid, for slices containing 100%, 80%, 20%, and 0.1% of the 0.218 A peak current, for the three cases shown in Figure 8. The dotted contours bound the areas of allowed trace space orientations for the 0.1% (green), 20% (red), and 80% (black) slices as calculated from Eq. (8). This plot shows that for matching solenoid locations of 4 cm (triangles) and 6.5 cm (circles) the endpoints fall within the corresponding curves indicating that the beam is well-confined, while the 14.5 cm case (squares) is not, in agreement with Figure 8.

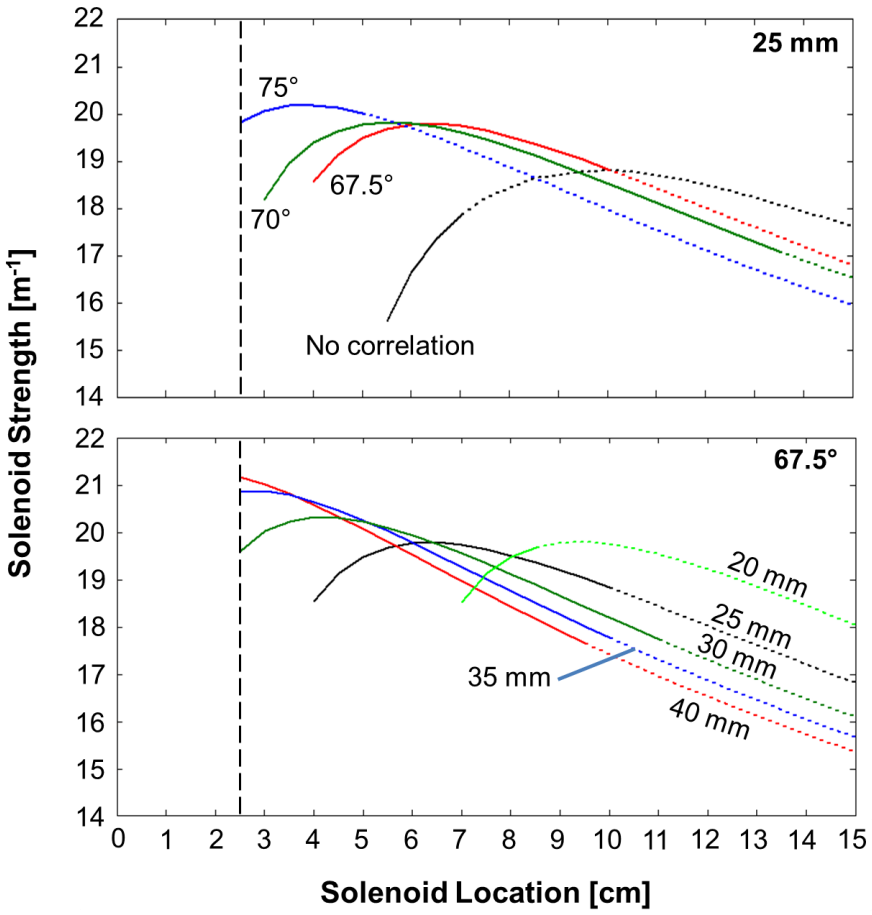

Figure 10. Matching solenoid strength (k_{sol}), as a function of position (l_{sol}), which is required to match the 10 keV, 0.218 A slice into a uniform linear focusing channel with a final radius of 5 mm, assuming initial conditions defined in Eqs. (1) and (2) and Tables I and II. Dotted lines are shown where the peak current slice was well-matched, but the beam was not well-confined, while solid lines are shown where the peak current slice was well-matched, and the beam was well-confined. Only gun geometries that exhibited well-confined beams for some combination of solenoid location and strength are shown in this figure. Smaller solenoid position step sizes were used at smaller distances to better resolve the curvature near the peak curves.